Inviscid Simulation of Various Internal Isoenergetic Compressible Flows

E. Y-K. NG
School of Mechanical and Production Engineering, Nanyang Technological University,Nanyang Avenue, Singapore 2263.

Abstract: To take full advantage of computational fluid dynamics (CFD) in the design of internal flow components such as the duct and turbomachinery blade rows, it is necessary to develop numerical methods that offer both accurate solutions for realistic flows and minimum turn-around time and computer cost. While a Navier-Stokes solver is really required for the above purpose, the problem of turbulence modeling and the large amount of CPU time make a fast and robust 2-D Euler code (with its simplicity in the method) still a desirable tool for routine applications. Results obtained from this prediction are particularly useful in preliminary design work where information on pressure alone is desired and for problems where the viscous / inviscid interaction is weak. An investigation on the numerical technique for Euler equations has been made and applied to internal flow problems on a VAX-9000 computer. Comparisons of various duct flows simulation were then performed between numerical calculations and well-documented experimental data. Their agreements are very encouraging. Preliminary results of both turbine and compressor flow computations were also conducted to illustrate the capability and limitations of these inviscid predictions. The time-marching strategy developed is based on Denton's finite volume algorithm. Time steps are not severely restricted when grid points are closely distributed. An outline of the scheme is addressed and the current applications of the solver are assessed.

Received : June 18,1995
Accepted : Sept. 14,1995

Keywords : *Inviscid, Isoenergetic Compressible Flows.*

INTRODUCTION

Time marching approaches for predicting internal flows have been developed for more than 34 years [1 and 2]. The main advantages of these schemes are their ability to calculate mixed supersonic and subsonic flows with automatic shock capturing beside their great simplicity and the physical understanding resulted from the solution procedure. The 2D and 3D Euler equations, though no viscous effects, are still widely applied in fluid machinery design and are almost

always solved by an explicit procedure. Methods for solving these equations are now highly developed with several different numerical algorithms being available. Implicit predictions have not proved more efficient than explicit ones for this application, particularly when the latter uses multigrid (though not implemented here) to accelerate the convergence.

The numerical procedure developed here is based on the time-marching method developed by Denton [3]. The basic principle involved is to begin with a guessed flow distribution and integrate the time dependent equations of motion and energy forward with time until a steady state solution is achieved. This finite volume integral method is claimed to be more stable than the differential approaches [2] as all fluxes are conserved and changes of momentum equate to the forces imposed by the boundaries once the steady state is reached.

The aim of the work is to demonstrate the capability of an Euler code to compute the entire flowfield. In the following sections, a brief outline will be given of the Euler solution procedure and then the solutions computed will be discussed and presented. Comparisons of the calculated results with an existing inviscid flow prediction and experimental data showed good agreement with differences being consistent with the existence of viscous effects.

MATHEMATICAL FORMULATION

Governing Equations

The 2-D Euler equations with Cartesian coordinate system in the differential form can be written as [3]:

Continuity
$$-\frac{\partial \rho}{\partial t} = \frac{\partial}{\partial x}(\rho V_x) + \frac{\partial}{\partial x}(\rho V_y) \tag{1}$$

X-momentum
$$-\frac{\partial (\rho V_x)}{\partial t} = \frac{\partial}{\partial x}(p + \rho V_x^2) + \frac{\partial}{\partial y}(\rho V_x V_y) \tag{2}$$

Y-momentum
$$-\frac{\partial (\rho V_y)}{\partial t} = \frac{\partial}{\partial x}(\rho V_x V_y) + \frac{\partial}{\partial y}(p + \rho V_x^2) \tag{3}$$

Energy $$-\frac{\partial(\rho E)}{\partial t} = \frac{\partial}{\partial x}(\rho V_x H) + \frac{\partial}{\partial y}(\rho V_y H) \quad (4)$$

By applying these equations for conservation of mass, momentum and energy to a series of control volumes with adjacent volumes sharing a common face and for a time step Δt and element of unit length with control volume ΔV, the Euler equations (1) - (4) become:

Continuity $$\Delta V \bullet \Delta\rho = \Delta t \bullet \Sigma n(\rho V_x \bullet dS_x + \rho V_y \bullet dS_y) \quad (5)$$

X-momentum $$\Delta V \bullet \Delta(\rho V_x) = \Delta t \bullet \Sigma n[(p + \rho V_x^2)\, dS_x + \rho V_x Vy \bullet dS_y)] \quad (6)$$

Y-momentum $$\Delta V \bullet \Delta(\rho V_y) = \Delta t \bullet \Sigma n[\rho V_x Vy \bullet dS_y + (p + \rho V_y^2) \bullet dS_y] \quad (7)$$

Energy $$\Delta V \bullet \Delta E = \Delta t \bullet \Sigma n(H\rho V_x \bullet dS_x + H\rho V_y \bullet dS_y) \quad (8)$$

The summations are made over the 4 faces of an element and dSx, dSy are the projections of the face in the x and y directions. That is, we are solving the equations (5) - (8) in integral form by applying the equations for conservation of mass, momentum and energy to a series of control volume with adjacent volumes sharing a common face. In this way once the steady state is reached the net flux into each elemental volume is zero so that overall mass and energy flows are conserved and changes of momentum equate to the forces imposed by the boundaries. The equations must be closed by an equation of state for the fluid which for a perfect gas would be P = ρRT. Since there is no heat flow and the viscous work terms in an inviscid fluid, provided that the flow is steady relative to the component being calculated and Prandtl number near unity, the energy equation reduces simply to the conservation of stagnation enthalpy (or rothalpy for rotor blades) along a streamline which is a well known steady flow energy equation from basic Thermodynamics. This assumption implies that energy is diffused by gradients of stagnation temperature rather than of static temperature such that the stagnation temperature is constant through an adiabatic boundary layer. This is known to be a good approximation for internal flow calculations except hypersonic flows. It is also much more efficient computationally as no exponentiation is needed in obtaining the pressure from the density via

$$T = (H - 0.5 * V^2)/C_p \quad \textit{and} \quad P = rRT \quad (9)$$

Numerical Solution Technique

A simple H-mesh is used due to its simplicity and flexibility. The time-marching method is applied to the H-grid consisting of quadrilateral elements which do not overlap and have nodes only at their corners which reduces finite differencing errors and allow complete freedom to vary the size of the elements. Both these factors help to improve entropy conservation. In the turbomachinery calculation, the quasi-streamlines upstream and downstream of the cascade are chosen to be roughly in line with the flow inlet and exit directions but these lines do not control the flow direction. Periodicity is applied over the bounding quasi-streamlines so that the boundaries exert zero force on the flow and do not control its direction. The outlet flow direction is predicted as part of the calculation being determined by the periodicity condition behind the trailing edge. The fluxes through the quasi-streamlines are usually small compared to those through the pitchwise lines and are obtained directly from the fluid properties at the calculating points on the streamwise faces of the elements.

The equations are solved in the order: mass-pressure-momentum. The procedure adopted is to update the density at all grid points then use the new density in conjunction with the old velocities to get the pressure at each grid point (Eq. (9)). Finally, the new pressures together with the old densities and velocities are applied to update the x-momentum and y-momentum. The order in which the momentum equations are solved is not important (i.e. an explicit scheme where the new variables are not used in the time step in which they are calculated with the exception that the new pressure is used immediately it is available). A stability analysis has been developed for the scheme by Denton [4] where the maximum permissible time step is $\Delta t_{max} = \Delta x_{min}[(\sqrt{M2+16}) - M] / 4c$.

To ensure stability, upwind differencing is adopted in the streamwise direction for fluxes of mass and momentum whilst downwind differencing is used for pressure. Central differencing is used for all quantities in the pitchwise direction. In the steady state, errors induced by upwind and downwind differencing are completely removed by the use of flux correction factors that correct the initial upwind and downwind flux estimates to accurate values based on any desired interpolation procedure. In other words, the basic philosophy of the marching scheme is to take a very simple and fast first-order scheme and progressively add on a second- or higher-order correction as the calculation converges. Details of this "Opposed Difference Technique" has been described in

[3] and has the useful property that its stability depends only on the axial Mach number, not on the absolute Mach number as is more usual.

The computer calculations for the complete program are very fast as virtually all operations are arithmetic. Time requirements are about 1.2×10^{-5} seconds per point per time step on VAX-9000. The number of time steps needed for convergence is depended by the number of grid points in the axial direction since the CFL condition requires that pressure waves cannot propagate more than one grid spacing per time step for an explicit method. For example, convergence to the steady state is achieved in 300-800 time steps for a (98x45) grid.

Boundary Conditions

With subsonic inflow the total temperature, total pressure and flow direction need be fixed at the upstream boundary whilst only the static pressure must be specified at the downstream boundary. With supersonic relative inflow, it is not usually possible to fix the flow direction and a condition of specified tangential velocity at inlet may be used instead. This permits the inlet flow direction to change as the calculation proceeds. The resulting solution will then satisfy the unique incidence condition to the blade row for cascade flow calculation. If the axial Mach number is greater than unity all flow conditions must be fixed at the upstream boundary because pressure waves can no longer reach it to change the inflow conditions. The static pressure at the upstream boundary must be obtained either by extrapolation from the interior flow field or by use of characteristics type relationships applied to upstream traveling pressure waves.

In brief, the boundary conditions applied at the downstream boundary are a specified uniform static pressure on the last pitchwise line and a condition of zero velocity gradient along the quasi-streamlines. At the upstream boundary the stagnation pressure and temperature and flow direction are specified and there is assumed to be no pressure gradient along the quasi-streamlines. The static pressure on the first pitchwise line is taken to be the same as that predicted on the same quasi-streamline at the second pitchwise line. This static pressure is used in conjunction with an assumption of isentropic flow from the stagnation conditions to calculate the velocity and density. The inlet flow is, thus, not necessarily uniform.

For the turbomachinery prediction, the periodicity condition on the "free" boundaries upstream and downstream of the blades is easily satisfied by considering points outside the calculation domain to have the same flow properties as points one pitch distant within the domain and then equating all flow properties at corresponding points on the boundaries.

COMPARISON OF FLOW PREDICTIONS TO SOME REPRESENTATIVE TEST CASES

Six test examples are included. We compare the calculation (for test cases 1, 2, 3 and 5) with others' data by keeping the flow Reynolds numbers of the computation equal to the analytical/experimental ones. The matching of flow condition is done through the proper scaling of flow geometry and only a qualitative (not quantitative) comparison is made here for test cases 2, 3 and 4.

The Circular-Arc S-Shaped Duct [5]

A simple but interesting test case is the non-diffusing (optimum), subsonic flow through a circular-arc S-shaped duct (59x7 H-mesh) in which each of the two arcs had equal centerline radii of curvature. The duct's two turns were completed in 45^0 and, thus it had an offset-to-length ratio, d/L, of approximately 0.414.

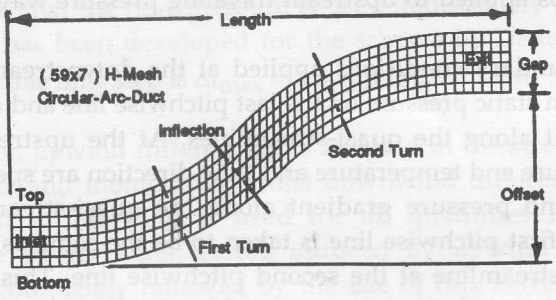

Figure 1 : Experimental Duct and Geometry Definitions.

The center-line radius of curvature was 508 mm for each of the turns and the gap* was 101.6 mm as illustrated in Figure 1. The flow Reynolds numbers is 6.56x104 based on the inlet condition and duct hydraulic diameter.

The predicted wall surfaces Cp's along the top and bottom walls of the duct and pressure, Mach number contours with streamlines velocity vector plots are depicted in Figure 2. Good agreement is achieved over most of the duct profile except near the rear part of the duct. In real flow, the major impact of viscous

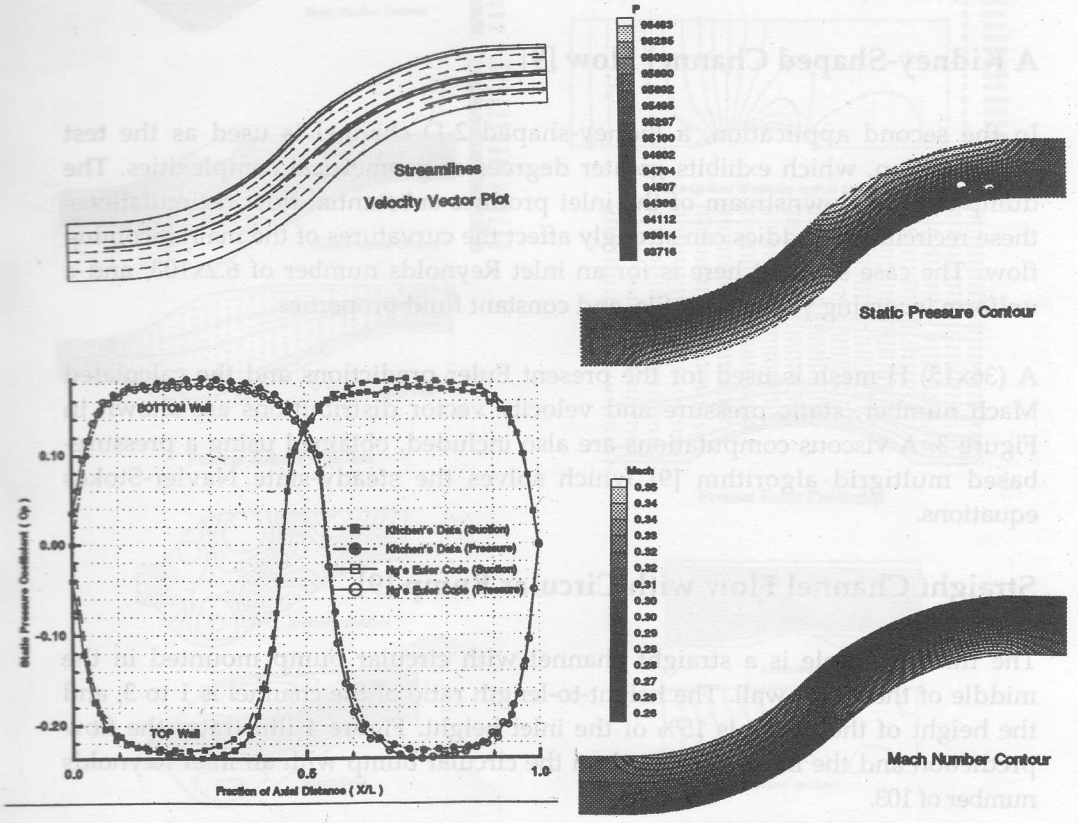

Figure 2: Predicted Flow Field Distributions for 45^0- 45^0 Circular-Arc-Duct.

---

* *Offset is defined as the cross-stream distance from inlet to exit centerlines whilst gap is defined as the constant radial spacing between the curved duct walls. The optimum duct implied that duct which was least prone to separation. Note that Truckenbrodt's boundary layer integral method (1973) was used in conjunction with a numerical potential flow program in reference [5].*

effects arises from the boundary layer blockage and if this can be modelled by coupling the Euler calculation with a separate boundary layer solution on the wall surfaces then improved results may be achieved [6]. However, many aircraft use bending rectangular and circular duct geometries in the inlet and exhaust of the propulsion systems. The performance of these types of ducts, which may have strong secondary flows and can have an adverse effect on the pressure distribution (i.e., cause high total pressure distortion) and on pressure recovery at the engine face, should be determined by full 3-D Navier-Stokes solver [7 and 8].

A Kidney-Shaped Channel Flow [9]

In the second application, a kidney-shaped 2-D channel is used as the test configuration, which exhibits greater degrees of geometrical complexities. The dump regions downstream of the inlet produce substantial flow recirculations; these recirculating eddies can strongly affect the curvatures of the main incoming flow. The case selected here is for an inlet Reynolds number of 6.2x103, and a uniform incoming velocity profile, and constant fluid properties.

A (36x15) H-mesh is used for the present Euler predictions and the calculated Mach number, static pressure and velocity vector distributions are shown in Figure 3. A viscous computations are also included, obtained using a pressure-based multigrid algorithm [9] which solves the steady-state Navier-Stokes equations.

Straight Channel Flow with Circular Bump [9]

The third example is a straight channel with circular bump mounted in the middle of the lower wall. The height-to-length ratio of the channel is 1 to 3, and the height of the bump is 15% of the inlet height. Figure 4 illustrates the flow prediction and the mesh employed on the circular bump with an inlet Reynolds number of 103.

Cylindrical and Elliptical Cascade

The next test case is the subsonic flow over a cascade of cylinders (65x51 H-cells) or ellipses (92x51 H-meshes). The blunt leading edge creates a very highly distorted mesh where numerical errors are expected to be large. These will then

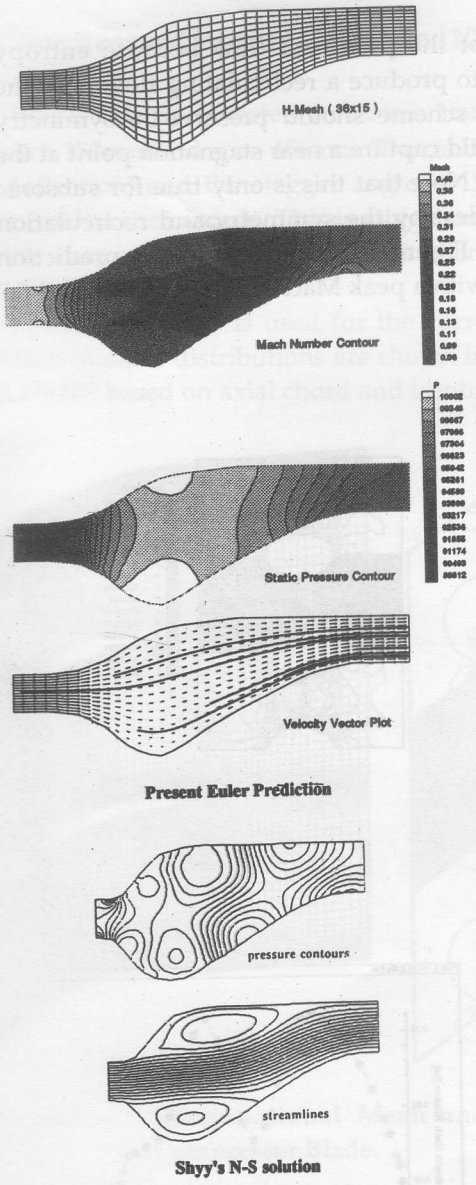

Figure 3 : Solutions of Kidney-Shaped Channel Flow with Re=6.2x10^3.

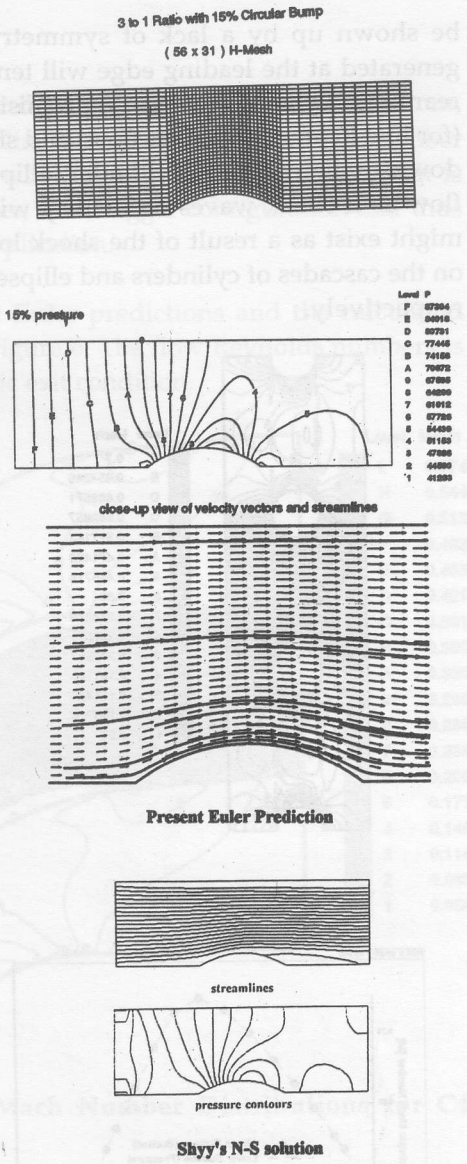

Figure 4 : Computed Flow Field in a Channel with 15% Circular Bump.

be shown up by a lack of symmetry of the predicted flow because entropy generated at the leading edge will tend to produce a recirculating flow near the rear of the cylinder/ellipse. A promising scheme should preserve the symmetry (for low Reynolds number flow) and should capture a near stagnation point at the downstream end of the cylinder/ellipse. Note that this is only true for subsonic flow as if shock waves occur they will destroy the symmetry and recirculation might exist as a result of the shock loss. Figure 5 illustrates the flow prediction on the cascades of cylinders and ellipses with a peak Mach number of 0.76 and 0.7 respectively.

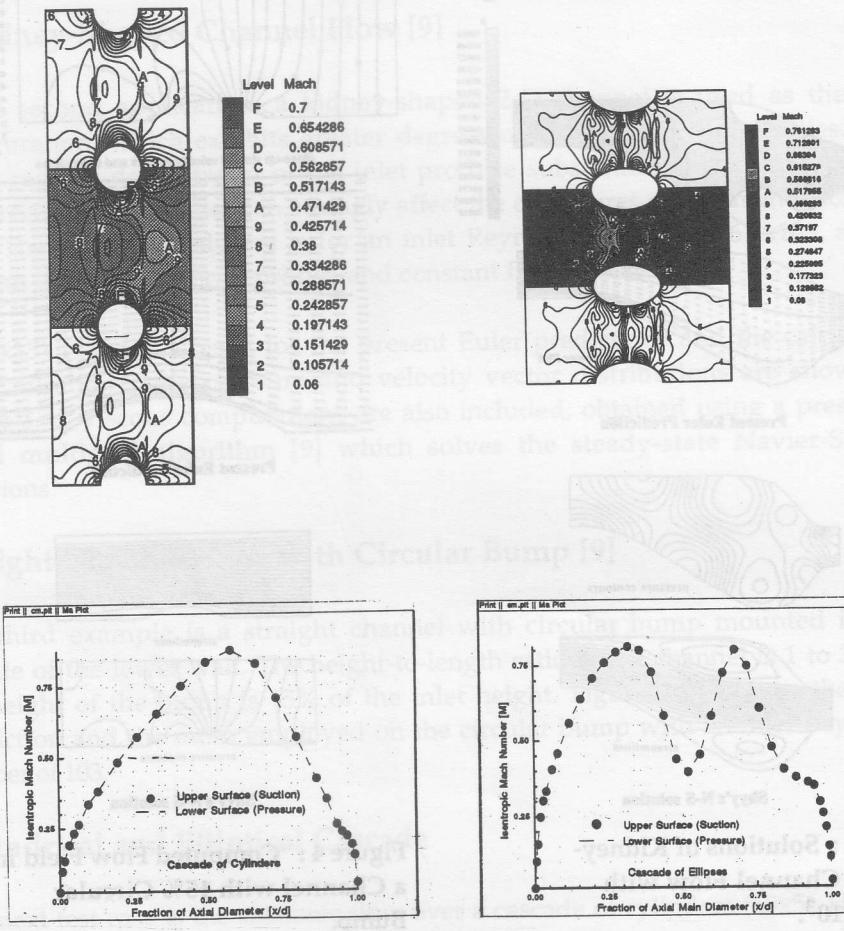

Figure 5: Computed Flow Around the Cascades of Cylinders and Ellipses.

Compressor Cascade C4-Blade [10]

The cascade to be tested consists a standard C4 section, each of chord 152mm, pitch 152mm and span 456mm. The camber line is a circular arc with 40° of camber (deflection) and the stagger angle is 15° when measured from a line which is normal to the cascade. This is a high camber, low stagger configuration and thus it is more suitable for low Mach number application.

A (98x45) H-mesh is used for the current Euler predictions and the calculated Mach number distributions are shown in Figure 6. The flow Reynolds numbers is 2.17×10^5 based on axial chord and isentropic exit condition.

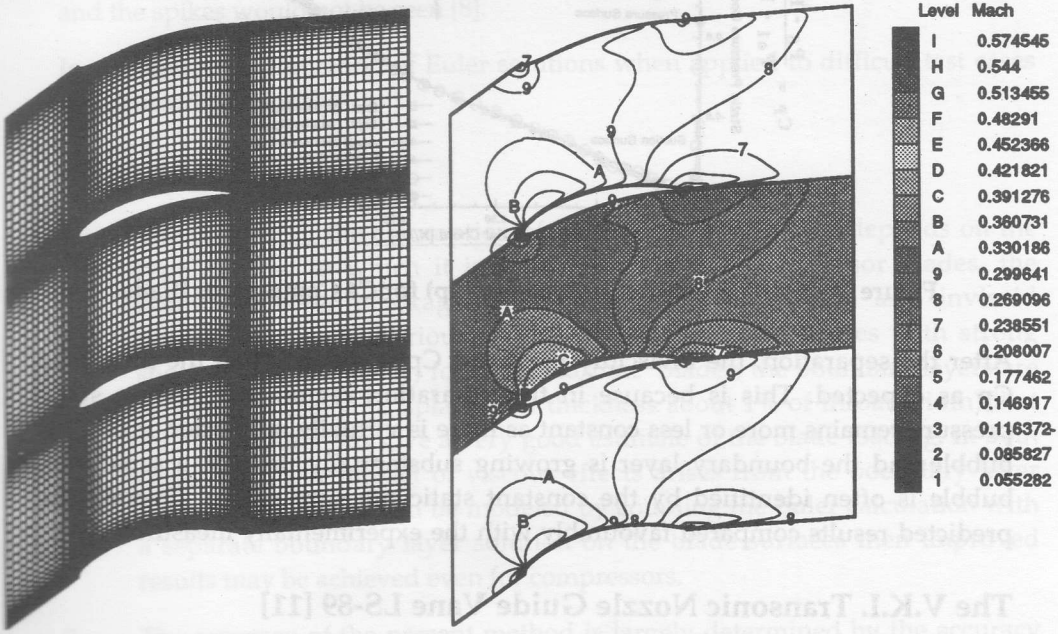

Figure 6 : Computational Mesh and Mach Number Distributions for C4 Compressor Blade.

Figure 7 compares the experimental and predicted blade Cp's. Other inviscid computations are also included, obtained using a finite element programme (Whitehead, 1982 [10]) which solves the potential flow equations. Near the leading edge of the suction side and toward the trailing edge (particularly on

pressure side), it may be seen that the inviscid values of Cp are higher than the measured value [10]. This is due to the absence of any viscous blockage effects in the inviscid calculation. The absence of blockage produces a larger effective flow area and higher average Cp values. However, these effects are not so noticeable on the leading edge of the pressure side as the initial curvature of the profile is comparatively small.

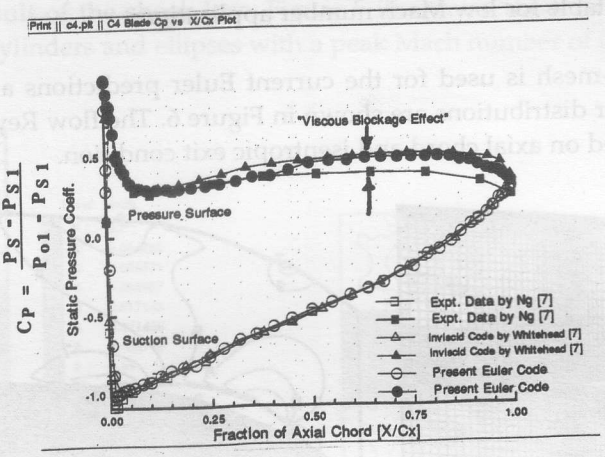

Figure 7 : Static Pressure Coefficients (Cp) for C4 Compressor Blade.

After the separation, the inviscidly predicted Cp is greater than the measured Cp as expected. This is because in the separation region, the surface static pressure remains more or less constant as there is virtually no motion inside the bubble and the boundary layer is growing substantially. In fact, a separation bubble is often identified by the constant static pressure region. Overall, the predicted results compared favourably with the experimentally measured data.

The V.K.I. Transonic Nozzle Guide Vane LS-89 [11]

The last test example is the blade profile similar to the one of VKI's highly loaded transonic linear turbine guide vane cascade LS-89 and the major specifications are given in [11].

Two operating modes were calculated for isentropic exit Mach numbers of 0.85 and 1.02 (125x49 H-cells) and then compared with both the measured Misent. and the inviscid solutions obtained by Holmes using a 2-D adaptive unstructured grid

Euler solver [11] as presented in Figures 8 and 9 respectively. Again, good agreement is achieved over most of the blade profile except near the rear part of the blade. The accuracy of inviscid computations on a cascade depend largely on -- high turning with a blunt trailing edge -- hangs entirely on the treatment of the trailing edge. We have chosen here to set a stagnation point at the node closest to the point where the blade mean line pierces the trailing edge circle. Within the realm of a purely Euler prediction, this is a very clean approach to the problem of blunt trailing edges, but it may not give the most realistic approximation to the true viscous solution. The strong accelerations and decelerations at the trailing edge are due to the fact that these are Euler calculations with the flow remaining attached at the blunt trailing edge. Note that a Navier-Stokes solution would show a flow separation at the trailing edge and the spikes would not be seen [8].

In summary, the limitation of Euler solutions when applied to difficult test cases is discussed previously.

CONCLUSIONS

1. The validity of the assumption of inviscid flow obviously depends on the type of flow to which it is being applied. For compressor blades, the boundary layer blockage is much larger than turbine and inviscid predictions can be seriously in error, especially for blades with strong shock waves. However, for most turbine blades, the boundary layers are so thin (typically displacement thickness about 1% of throat width) that Euler computations give a very good estimate of the blade loading. In both cases the major impact of viscous effects arises from the boundary layer blockage and if this can be modeled by coupling the Euler calculation with a separate boundary layer solution on the blade surfaces then improved results may be achieved even for compressors.

2. The accuracy of the present method is largely determined by the accuracy of the finite differencing employed on the solid surfaces (i.e. for the implementation of boundary condition). In the cascade flows, the rates of change of fluid properties are largest around the leading edge of a blade therefore, in order to minimize differencing errors, a much finer mesh is desirable in this region. Also, some reduction of pitchwise grid spacing is beneficial near to all solid boundaries so as to reduce the errors due to one sided differencing.

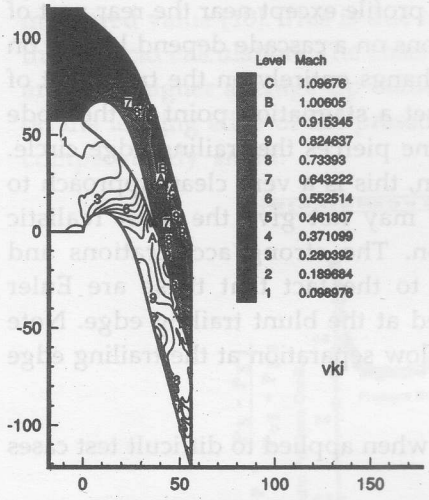

Present Euler Solver

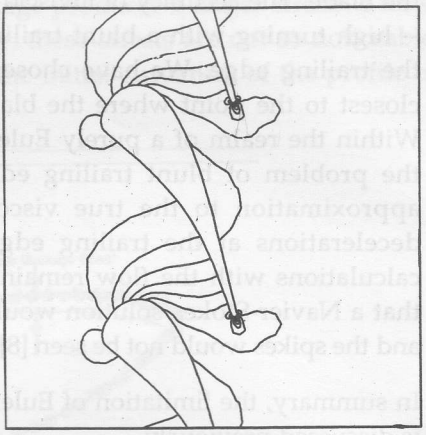

Holmes's Inviscid Code

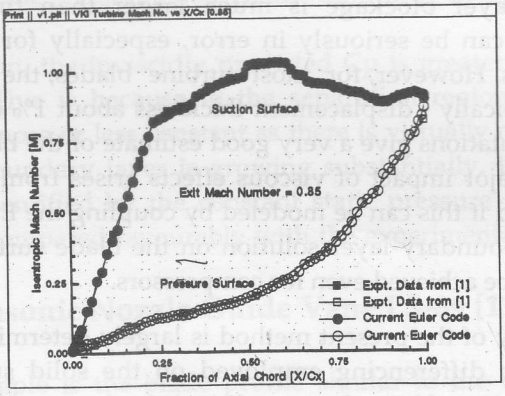

Figure 8 : Comparison of Mach Number Distribution with Isentropic Exit Mach Number of 0.85 for Turbine Nozzle Guide Vane.

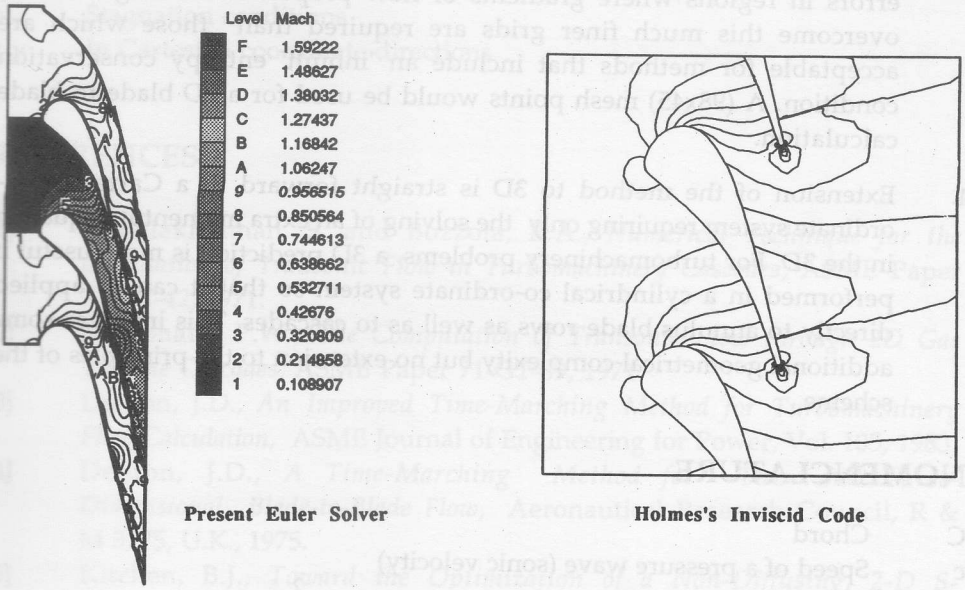

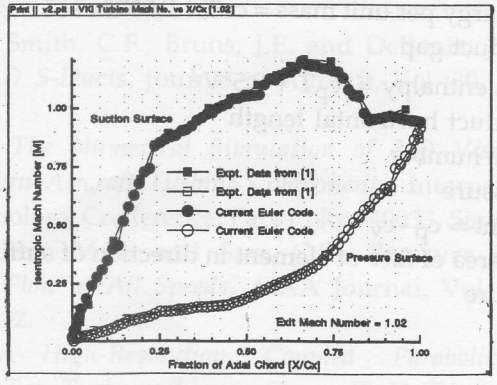

Figure 9 : Comparison of Mach Number Distribution with Isentropic Exit Mach Number of 1.02for Turbine Nozzle Guide Vane.

3. Limitations on accuracy occur due to false entropy generation by numerical errors in regions where gradients of flow properties are large, and to overcome this much finer grids are required than those which are acceptable for methods that include an 'inbuilt' entropy conservation condition. A (98x45) mesh points would be used for a 2D blade to blade calculation.

4. Extension of the method to 3D is straight forward in a Cartesian co-ordinate system requiring only the solving of an extra momentum equation in the 3D. For turbomachinery problems, a 3D prediction is more useful if performed in a cylindrical co-ordinate system so that it can be applied directly to annulus blade rows as well as to cascades. This involves some additional geometrical complexity but no extension to the principles of the scheme.

NOMENCLATURE

C	Chord
c	Speed of a pressure wave (sonic velocity)
Cp	Static pressure coefficient = $(P_s-P_{o1}) / 0.5*\rho *V_1^2$
Cp,Cv	Specific heat of const. pressure & volume respectively
d	S-shaped duct offset
E	Internal energy per unit mass = $cvT + 0.5*V^2$
g	S-shaped duct gap
H	Stagnation enthalpy = $c_pT + 0.5*V^2$
L	S-shaped duct horizontal length
M	Local Mach number
P	Static pressure
R	Gas constant = $c_p - c_v$
S	Projected area of face of element in direction of suffix
T	Temperature
Δt	Time step
V	Velocity
ΔV	Volume of element
ρ	Fluid static density

Suffices:

o	Stagnation conditions
x,y	In Cartesian coordinate directions

REFERENCES

[1] Gopalakrishnan, S. and Bozzola, R.A., *Numerical Technique for the Calculation of Transonic Flow in Turbomachinery Cascades*, ASME Paper 71-GT-42, 1971.

[2] McDonald, P.W., *The Computation of Transonic Flow through 2D Gas Turbine Cascades*, ASME Paper 71-GT-89, 1971.

[3] Denton, J.D., *An Improved Time-Marching Method for Turbomachinery Flow Calculation*, ASME Journal of Engineering for Power, Vol. 105, 1983.

[4] Denton, J.D., *A Time-Marching Method for Two- and Three-Dimensional Blade-to-Blade Flow*, Aeronautical Research Council, R & M 3775, U.K., 1975.

[5] Kitchen, B.J., *Toward the Optimization of a Non-Diffusing, 2-D S-Shaped Duct*, Ph.D. Thesis, The Wichita State University, U.S.A., 1989.

[6] Lee, D. and Pletcher, R.H., *Simultaneous Viscous-Inviscid Interaction Calculation Procedure for Transonic Turbulent Flows*, AIAA Journal, Vol. 26, No: 11, Page 1354 - 1362, 1988.

[7] Harloff, G.J., Smith, C.F., Bruns, J.E. and DeBonis, J.R., *Navier-Stokes Analysis of 3-D S-Ducts*, Journal of Aircraft, Vol. 30, No: 4, Page 526 - 533, 1993.

[8] Ng, E. Y-K., *The Numerical Simulation of 3-D Viscous Compressible Flow for Modern Aircraft Turbine Components*, International Pacific Air & Space Technology Conference, Paper No: 940033, Singapore, 1994.

[9] Shyy, W., Chen, M.H. and Sun, C.S., *Pressure-Based Multigrid Algorithm for Flow at All Speeds*, AIAA Journal, Vol. 30, No: 11, Page 2660 - 2669, 1992.

[10] Ng, E. Y-K. *A High-Resolution Coupled Parabolic / Elliptic Navier-Stokes Solver For Turbomachinery Flows*, Ph.D Thesis, University of Cambridge, U.K. 1992.

[11] Art, T., Sieverding, C.H. et al. *Numerical Methods for Flows in Turbomachinery*, V.K.I. Lecture Series-06, von Karman Institute for Fluid Dynamics, Belgium, 1989.